PCCP

PAPER

CrossMark
click for updates

Understanding of matrix embedding: a theoretical spectroscopic study of CO interacting with Ar clusters, surfaces and matrices†

K. Mahjoubi,[a] D. M. Benoit,*[b] N.-E. Jaidane,[a] M. Mogren Al-Mogren[c] and M. Hochlaf*[d]

Through benchmark studies, we explore the performance of PBE density functional theory, with and without Grimme's dispersion correction (DFT-D3), in predicting spectroscopic properties for molecules interacting with rare gas matrices. Here, a periodic-dispersion corrected model of matrix embedding is used for the first time. We use PBE-D3 to determine the equilibrium structures and harmonic vibrational frequencies of carbon monoxide in interaction with small Ar clusters (CO–Ar$_n$, n = 1, 2, 3), with an Ar surface and embedded in an Ar matrix. Our results show a converging trend for both the vibrational frequencies and binding energies when going from the gas-phase to a fully periodic approach describing CO embedding in Ar. This trend is explained in terms of solvation effects, as CO is expected to alter the structure of the Ar matrix. Due to a competition between CO–Ar interactions and Ar–Ar interactions, perturbations caused by the presence of CO are found to extend over several Å in the matrix. Accordingly, it is mandatory to fully relax rare gas matrices when studying their interaction with embedded molecules. Moreover, we show that the binding energy per Ar is almost constant (~ -130 cm^{-1} atom^{-1}) regardless of the environment of the CO molecule. Finally, we show that the concentration of the solute into the cold matrix influences the spectroscopic parameters of molecules embedded into cold matrices. We suggest hence that several cautions should be taken before comparing these parameters to gas phase measurements and to theoretical data of isolated species.

I. Introduction

Matrix isolation is used as a tool for the characterization of stable and "unusual" molecular systems, such as radicals, ions, *etc.* In 1954, Pimental and Charles[1] pointed out that observations in matrix experiments displayed bands shifted from their gas-phase counterparts. Afterwards, several investigations, both theoretical and experimental, were performed in order to measure and to model the effects of matrix embedding. In addition, these studies tried to rationalize the observed deviations in the rotational and vibrational spectroscopic parameters that occurred upon complexation.

[a] *Laboratoire de Spectroscopie Atomique, Moléculaire et Applications – LSAMA, Université de Tunis El Manar, Tunis, Tunisia*

[b] *Department of Chemistry, University of Hull, HU6 7RX, UK. E-mail: D.Benoit@hull.ac.uk*

[c] *Chemistry Department, Faculty of Science, King Saud University, P.O. Box 2455, Riyadh 11451, Kingdom of Saudi Arabia*

[d] *Université Paris-Est, Laboratoire Modélisation et Simulation Multi Echelle, MSME UMR 8208 CNRS, 5 bd Descartes, 77454 Marne-la-Vallée, France. E-mail: hochlaf@univ-mlv.fr*

† Electronic supplementary information (ESI) available. See DOI: 10.1039/c5cp01672j

Briefly, these deviations are viewed as matrix induced perturbations on the structural parameters with respect to isolated (gas phase) molecular species. The recent PCCP perspective by Barone, Biczyskoa and Bloino,[2] for example, gives a detailed presentation of some molecular examples under conditions ranging from gas phase to low-temperature rare-gas matrices and helium nano-droplets.

In 1965, Friedmann and Kimel[3] proposed a simple model to explain the shifts of vibration–rotation lines of molecules in noble gas matrices. They showed the importance of intermolecular interaction forces between these molecules and rare gas matrices. Later on, Gerber and co-workers developed and applied the vibrational self-consistent field (VSCF) method for quantitative calculations of molecular vibrational spectroscopy in a crystalline solid environment. This method was successfully applied, for instance, for I@Ar$_n$ and HCl@Ar$_n$ systems.[4,5] Nevertheless, the main critical point is the accurate description of the interacting potentials.

Theoretically, noble gas matrix effects were considered within the framework of a polarizable continuum model[6,7] or empirically.[8] More sophisticated methods were recently proposed: for instance, the hybrid quantum-classical simulations by Niimi *et al.*[9]

They employed high-level *ab initio* calculations at the CCSD(T) level to construct interaction potential energy surfaces between embedded molecules and noble-gas atoms together with a Monte Carlo sampling of the molecule–noble gas configurations. Such electronic treatments remain however costly. Interestingly, all these studies highlighted the necessity of the explicit treatment of matrix environments around the embedded molecules to reproduce the experimentally observed vibrational shifts.

The prediction of reliable interacting potentials, including electrostatic, dispersion and induction effects, for embedded systems has been the focus of a number of theoretical and experimental investigations.[10,11] In this study, we use a unified first-principles methodology for all environments (gas phase clusters and molecules adsorbed on a rare-gas surface or embedded into a rare-gas matrix) to derive these interaction potentials and afterwards the vibrational and structural effects caused by clustering and embedding. Moreover, we include dispersion effects in our solid-state calculations, as these are important for accurate derivations of the interaction potentials. As a benchmark system for our approach, we study the carbon monoxide molecule interacting with argon clusters or embedded into a cold Ar matrix. The choice of carbon monoxide, CO, is motivated by its importance in several physical, chemical and biological processes and also due to its abundance in the universe. For instance, it is an important basic chemical for the production of many other compounds such as polycarbonate and acetic acid,[12] or in a number of reactions in humans.[13] Argon in the form of clusters or matrices is an ideal solvent model as it interacts with CO mainly through van der Waals (vdW) forces, and the relatively limited size of the system allows us to use elaborate theoretical treatments.

Isolated CO ($X^1\Sigma^+$) has been extensively studied both experimentally and theoretically (see for instance ref. 14–17). The interaction of CO with rare-gas atoms has also been the subject of numerous theoretical studies.[18–20] However, most studies that used elaborate *ab initio* methodologies (*e.g.* coupled cluster with singles, doubles, and non-iterative triples, CCSD(T)[21]) were limited to exploring the interaction of CO with a relatively small number of rare-gas atoms (mainly two or three atoms). This is due to the computational cost of high-level methods. Indeed, increasing the number of rare-gas atoms in such systems leads to a very significant increase in computational cost for highly correlated methods, mainly due to the large basis sets necessary for describing the long range interactions.

In this study, we compute the structures and the vibrational spectra of CO either attached to small Ar clusters (CO–Ar_n, $n = 1$, 2, 3), or interacting with an Ar surface or embedded into a cold Ar matrix. After benchmarking our technique, we show the efficiency of PBE-D3 in treating these molecular systems. As stated by Havenith and Schwaab,[22] Ar–CO exhibits portions of attractive components: electrostatics/induction/dispersion in a ratio of 1.3/1.4/8.3. This partitioning demonstrates the dominance of dispersion energy[23] in CO–Ar_n systems. Thus, CO–Ar and larger clusters are ideal test candidates for the study of dispersion effects and for the validation of theoretical approaches focusing on dispersion forces. Finally, we discuss the argon-induced shifts in the equilibrium geometry and in the vibrational frequency of CO.

Our paper is arranged as follows: we briefly describe the computational details in Section II. Our results for CO–Ar_n are presented in Section III and Section IV contains the results obtained for CO adsorbed on Ar surfaces and embedded in an Ar matrix. We discuss our findings in Section V and present our conclusions in Section VI.

II. Computational details

1. *Ab initio* calculations

In order to describe the electronic structure of the CO–Ar_n clusters, we used Møller–Plesset second-order perturbation theory (MP2),[24–26] the complete active space self-consistent field (CASSCF) technique,[27,28] with a full valence active space, followed by an internally contracted Multi Reference Configuration Interaction (MRCI) approach,[29,30] and the standard[31,32] (CCSD(T)) and explicitly correlated (CCSD(T)-F12)[33] coupled cluster approaches including perturbative triple corrections. These computations are performed using the MOLPRO (version 2012)[34] and the GAUSSIAN 09[35] package. In these computations, the atoms were described using Dunning and co-workers' aug-cc-pVTZ and aug-cc-pVQZ basis sets.[36–39] For the explicitly correlated computations, we used in addition the corresponding auxiliary basis sets and density fitting functions[40,41] (*i.e.*, the default CABS(OptRI) basis sets of Peterson and co-workers[42] as implemented in MOLPRO). This approach is validated for the computations of vdW interactions.[43–45]

2. Density functional theory calculations

Recent developments in density functional theory (DFT)[46] improved our ability to account correctly for vdW interactions.[47] For instance, DFT has been used to describe the CO–Mg_nO_n ($n = 5$–25)[48] and CH_3O–Cu_{22}[49] clusters. However, while DFT is nominally an exact theory, it has shown a number of limitations in the treatment of dispersion interaction[50,51] – a particularly acute issue for systems containing rare gas atoms and periodic systems.[52] Savin and co-workers[53] proposed a composed alternative scheme where they coupled DFT and MP2.[24] This approach is viewed as a good solution for small systems since it circumvents the dispersion problem for rare gas dimers.[54] Nevertheless, the application of DFT-based methodologies in this context remains limited.

Here, the DFT calculations were performed using the Quickstep[55] module of the CP2K program package version 2.3,[56] where we treated explicitly the valence electrons while the core electrons are described using norm-conserving Goedecker–Teter–Hutter (GTH) pseudo-potentials.[57] We used the Perdew–Burke–Ernzerhof (PBE)[58] exchange correlation functional along with a molecularly optimized triple-zeta valence basis set with one polarization function (TZVP-MOLOPT-GTH) for carbon and oxygen and the TZV2P-GTH basis set for argon.[59,60] In order to remove any basis-set superposition error (BSSE),[61] we also used the much larger basis sets, QZV2P-GTH for C and O and

17160 | *Phys. Chem. Chem. Phys.,* 2015, **17**, 17159–17168

This journal is © the Owner Societies 2015

QZV3P-GTH for Ar. The plane-wave cut-off energy for calculations on clusters, surfaces and matrices is fixed at 400 Ry and the wave functions are converged to less than 10^{-7} Hartrees. Geometries were optimised using the Broyden–Fletcher–Goldfarb–Shanno (BFGS) method with a tolerance of 10^{-4} H per bohr for MAX_DR and 10^{-6} H per bohr for MAX_FORCE.

The cell size varies according to the type of calculation performed: for clusters we use a cubic cell of 20 Å in length, while the periodic systems use a multiple of an optimised face centred cubic (fcc) argon crystal with a lattice constant equals to 5.2229 Å (see details in Section IV).

Aziz and co-workers established the importance of considering dispersion interaction for Ar_n containing clusters.[62] Recently, Grimme and co-workers[52] proposed an empirical correction technique that includes the effects of dispersion interactions in DFT calculations. The technique called DFT-D (density functional theory with empirical dispersion corrections) is now a popular approach and has recently been refined to account for different bond types (DFT-D3).[52] For the first time, we used the DFT-D3 empirical vdW correction proposed by Grimme and co-workers, where the total energy in this approach is given by the sum of the DFT total energy and the van der Waals correction:

$$E_{\text{tot}} = E_{\text{DFT}} + E_{\text{disp}} \tag{1}$$

as implemented in CP2K.

Binding energies (E_B) were calculated using the supermolecule approach and corrected for BSSE using the procedure suggested by Boys and Bernardi.[61]

III. CO–Ar_n (n = 0, 1, 2, and 3) clusters

1. Isolated CO

To better understand the environment effects of rare-gas embedding on the carbon monoxide, we first determine the spectroscopic properties of isolated CO in its electronic ground state ($X^1\Sigma^+$). The results and their comparison to experimental data are listed in Table 1. This table shows that all levels of theory, except MRCI/aug-cc-pVQZ, lead to ~0.01 Å deviations from the experimental equilibrium distance. We note that both PBE-D3/QZV2P and PBE/TZVP provide the same distance (1.138 Å). For the harmonic frequency, the MP2/aug-cc-pVTZ value is relatively far away from experimental data. Interestingly, the harmonic

Table 1 Equilibrium distance and vibrational frequency of carbon monoxide

Method/basis set	r_e/Å	$|r_e - r_e^{\text{Exp}}|$/Å	ω_e/cm^{-1}	$|\omega_e - \omega_e^{\text{Exp}}|$/cm^{-1}
MP2/aug-cc-pVTZ[a]	1.139	0.011	2110.0	59.8
PBE/TZVP[b]	1.138	0.010	2134.0	35.8
PBE-D3/TZV2P[a]	1.137	0.009	2153.5	16.3
PBE-D3/QZV2P[a]	1.138	0.010	2142.8	27.8
CCSD(T)/aug-cc-pVTZ[a]	1.135	0.007	2144.61	25.2
CCSD(T)-F12/aug-cc-pVTZ[a]	1.130	0.002	2161.43	8.4
MRCI/aug-cc-pVQZ[a]	1.130	0.002	2155.9	13.9
CCSD(T)/aug-cc-pVQZ[b]	1.125	0.011	2160.0	9.8
Experimental[c]	1.128	—	2169.8	—

[a] This work. [b] Ref. 80. [c] Ref. 81.

frequency obtained with PBE-D3/TZV2P is only 16 cm^{-1} away from experimental data, improving on MP2/aug-cc-pVTZ and PBE/TZVP, and of a similar quality to the MRCI/aug-cc-pVQZ values. Yet, increasing the size of the basis set to PBE-D3/QZV2P yields a much lower frequency (28 cm^{-1} away from experimental data), thus indicating a possible fortuitous error cancellation for TZV2P. The CCSD(T)/aug-cc-pVQZ harmonic vibrational frequency is reassuringly close to the experimental harmonic value. As expected the CCSD(T)-F12/aug-cc-pVTZ harmonic frequency is close to the CCSD(T)/aug-cc-pVQZ value, whereas the CCSD(T)-F12 equilibrium distance is closer to experimental data. This validates the use of the CCSD(T)-F12/aug-cc-pVTZ level as reference for CO–Ar_n clusters.

2. CO–Ar

In their review, Havenith and Schwaab[22] showed that the CO–Ar complex is an archetype molecular system to study weak intermolecular forces. For this reason, it has been widely investigated both experimentally and theoretically (we refer the readers to Havenith and Schwaab's review[22] and to the recent paper by Sumiyoshi and Endo[63] for further details).

In this study, we use different levels of electronic structure theory (MP2/aug-cc-pVTZ, CCSD(T)/aug-cc-pVTZ, CCSD(T)-F12/aug-cc-pVTZ and PBE-D3/TZV2P) to search for the stationary points on the ground-state potential of CO–Ar. Our results are shown in Table 2 together with a number of published values obtained using model potentials and various levels of electronic structure theory and the known experimental values. In order to facilitate the characterization of the geometry of this complex, we used the Jacobi coordinates where r_e is the CO distance, R corresponds to the distance between the centre of mass of CO and the Ar atom and θ is the angle between the CO axis and the R vector (where the Ar–CO arrangement corresponds to $\theta = 0°$). Note that Table 2 contains BSSE corrected binding energies (E_B).

At all levels of theory, we found three stationary points: two minimum structures, denoted as minimum 1 and minimum 2, and one transition state, denoted as the transition state, that connects both minima. These stationary points have been determined by geometry optimizations of the complex using different starting positions of the rare gas atom around the CO molecule. All three stationary points can be found on the semi-empirical potential reported in the review of Havenith and Schwaab (*cf.* Fig. 10 of ref. 22).

Table 2 reveals that our computed equilibrium parameters are in satisfactory agreement with the present and the published high-level calculations of both MP2 and PBE-D3. However, it is worth noting that PBE-D3 overestimates noticeably the binding energy for minimum 1. It is worth noting that the explicitly correlated CCSD(T)-F12 binding energies agree quite well with the semi-empirical values.
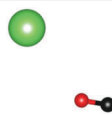
3. CO–Ar_2

For this system, the geometry optimisation leads to three structures: two minima and one transition state. These structures are depicted in Table 3, together with their geometrical parameters, BSSE corrected binding energies (E_B) and harmonic frequencies.

Table 2 Stationary points on the ground potential energy surface of CO@Ar. r_e, R_e and θ are the Jacobi coordinates. Distances are in Å, and angles in degrees. We give also the harmonic vibrational frequencies of the CO–Ar complex (ω_i, cm^{-1}) and the binding energy (E_B, cm^{-1}). See the text for more details. In bold are the CO harmonic frequencies. All computations were performed using the aug-cc-pVTZ basis set

	Minimum 1									Transition State			Minimum 2			
	MP2[a]	MP4[b]	CCSD(T)[c]	HHDSD/cc-pVQZ[d]	Semi-emp. Fit[e]	PBE-D3	MP2	CCSD(T)	CCSD(T)-F12	MP2	CCSD(T)	CCSD(T)-F12	MP2	CCSD(T)	CCSD(T)-F12	Semi-emp. Fit[e]
r_e						1.138	1.139	1.136	1.131	1.1389	1.136	1.1310	1.139	1.136	1.1301	
R_e	4.00	3.74	3.71	3.82	3.74	3.827	3.718	3.772	3.724	3.4572	3.5253	3.5199	3.449	3.505	3.514	4.78
θ	100	82	93	99	98	81.0	81.8	90.1	81.7	132.4	132.3	128.2	174.5	174.6	175.0	180
E_B	−69	−96	−105	−90	−100	−155.1	−128.7	−116.9	−103.1	−125.1	−107.9	−89.4	−125.5	−92.2	−94.6	−93
ω						**2150.6**	**2109.3**	**2144.33**	**2161.4**	**2108.7**	**2144.19**	**2160.59**	**2108.5**	**2144.13**		
						411.0	37.7	34.58	35.37	39.3	33.14	37.56	29.8	39.62		
						61.4	15.6	18.79	9.41	i4.2	i38.74	i7.73	5.3	20.95		

[a] Ref. 82. [b] Ref. 83. [c] Ref. 19. [d] Ref. 84. [e] Ref. 22.

E_B in this case is the BSSE-corrected energy difference between the complex, an isolated CO molecule and two isolated argon atoms.

The global minimum (minimum 1) corresponds to a structure where both argons are close to each other, in good agreement with the optimised geometry shown in Fig. 11 of ref. 47. The structure of minimum 2, which has not been reported previously, shows the CO sandwiched between both Ar atoms.
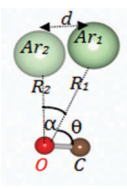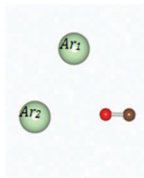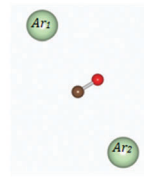
For the transition state, we see that both Ar atoms are closer to the CO fragment (about 3.4 Å) than for the two minima (about 3.7 Å in each minimum). We also note that the Ar–Ar distance is smaller in the transition state than in either

minimum 1 or minimum 2 and the oxygen of the CO molecule is pointing towards the centre of mass of an "Ar dimer".

Table 3 also shows that the influence of the interaction of CO with the argon dimer on the C–O distance is almost negligible. However, this is not the case with the harmonic vibration frequency of CO, as it decreases by ∼6.5 cm^{-1} with respect to the isolated carbon monoxide.

Finally, it is worth noting that PBE-D3 leads to shorter intermonomer distances than those obtained using MP2, but is in close agreement with the structures obtained with CCSD(T)-F12. Thus we expect a more compact cluster. This is in line with PBE-D3 overestimating the binding of CO–Ar. Nevertheless, this

Table 3 Equilibrium structures of the CO–Ar$_2$ complex. We give also the definition of the internal coordinates used for the characterization of these structures. Distances are Å, angles in degrees and harmonic vibrational frequencies (ω) and binding energies (E_B) are in cm^{-1}. In bold are the CO harmonic frequencies. The atoms were described using the aug-cc-pVTZ basis set. All computations were performed using the aug-cc-pVTZ basis set

	Minimum 1			Transition state		Minimum 2	
				θ=Ar$_1$ÔC, α= Ar$_1$ÔAr$_2$		θ=Ar$_1$ÔC, α= Ar$_1$ÔAr$_2$	
	PBE-D3	MP2	CCSD(T)-F12	MP2	CCSD(T)-F12	MP2	CCSD(T)-F12
r	1.1366	1.1390	1.131	1.1391	1.131	1.139	1.131
R_1	3.5424	3.7222	3.721	3.4779	3.533	3.777	3.733
R_2	3.5122	3.7321	3.678	3.4451	3.611	3.777	3.733
d	3.9045	4.7888	3.799	3.7595	4.165	7.354	6.911
θ	122.3	80.2	81.1	116.9	112.3	76.7	74.3
α	67.2	60.6	61.8	65.8	68.1	153.5	150.7
E_B	−274.3	−262.3	−202.8	−250.0	−192.0	−154.6	−171.1
ω	**2147.1**	**2108.9**		**2107.7**		**2109.0**	
	442.8	46.1		45.67		54.9	
	381.2	33.3		35.2		25.0	
	128.9	30.5		29.8		23.3	
	47.7	20.8		5.5		4.5	
	29.0	15.3		i3.0		3.4	

effect is mitigated here by the presence of an extra Ar molecule since the PBE-D3 binding energy of minimum 1 is closer to that obtained with MP2. We also note that for minimum 1 at the PBE-D3 level of theory, both the Ar1–O–Ar2 angle ($\alpha = 67°$) and the Ar–O–C angle ($\theta = 122°$) are larger than the value obtained with MP2 ($\alpha = 61°$ and $\theta = 80°$). Those values seem to indicate a much softer angular dependence of the PBE-D3 potential and are perhaps closer to the angles obtained for the transition state at the MP2 level.

4. CO–Ar$_3$

After geometry optimizations, we find two minimum structures (minimum 1 & minimum 2) and one transition state (transition state). The geometrical parameters of these structures are detailed in Table 4. Similarly to the optimised structure shown in Fig. 11 of ref. 47, the most stable minimum (minimum 1) shows that a triangle of Ar atoms above the CO molecule with a total binding energy of about -320 cm^{-1} is computed at the MP2/aug-cc-pVTZ level. In contrast to this, for both the transition state and minimum 2 the CO molecule is embedded into the Ar$_3$ cluster, *i.e.* CO and Ar atoms share the same plane. The Transition state and minimum 2 are less stable than minimum 1. They are located in potential wells, respectively, of -154 cm^{-1} (-193 cm^{-1}) and -173 cm^{-1} (-209 cm^{-1}) in depth at the MP2 (CCSD(T)-F12) level. Note that CO–Ar (minimum 1 & minimum 2),

CO–Ar$_2$ (minimum 2) and CO–Ar$_3$ (minimum 2) possess close binding energies. Their structures correspond roughly to a CO surrounded by Ar atoms, which belong to the first solvation shell of embedded CO into clusters. This work should give hence some information on the formation of the first solvation shell around the CO solute.

In minimum 1, the dihedral angles, which separate the planes containing the atoms of our system, are $\sim 34°$ and $\sim -69°$. These two angles become $0°$ and $180°$ for minimum 2 and both $0°$ for the transition state. For minimum 1, the Ar–O–Ar angles (α_1 and α_2) are similar for both methods ($\sim 68°$ for PBE-D3 and $\sim 63°$ for MP2), but there is again a marked difference between PBE-D3 and MP2 in the Ar$_1$–O–C angle (θ) as seen previously for the CO–Ar$_2$ complex.

Based in our calculations, the frequency shift of CO upon clustering with Ar$_3$ is ~ 8 cm^{-1}. Thus, ω_{CO} continues to decrease as we increase the number of argon atoms in the cluster. Note that these variations are more pronounced with PBE-D3 than with MP2.

IV. Periodic calculations

Our calculations on the CO–Ar$_n$ clusters show that PBE-D3/TZV2P is an efficient method to determine the electronic structure of carbon monoxide either isolated or in interaction with Ar. As an example for the Ar$_2$ dimer, we obtain an equilibrium distance of 3.860 Å with PBE-D3/TZV2P and 3.756 Å with MP2/aug-cc-pVTZ. Both values agree well with the experimental value of 3.756 Å.[64] Our computed BSSE-uncorrected binding energy for the Ar dimer is -126.63 cm^{-1} (PBE-D3/TZV2P) and -111.75 cm^{-1} (MP2/aug-cc-pVTZ), which are both over-estimating the value calculated at the CCSD(T)/aug-cc-pVQZ level of theory (-93 cm^{-1}).[62,65] However, PBE-D3 leads to a significant reduction of the computational cost compared to wave function based methodologies (*e.g.* MP2, CCSD(T)...) and theoretically allowing us to consider much larger systems. Thus, we suggest that PBE-D3 is of suitable accuracy for the study of CO deposited on Ar surfaces or embedded in Ar cold matrices. To the best of our knowledge, there are no applications of periodic local-MP2 to CO embedded into rare gas matrices.

1. Pure Ar crystals

We consider a pure argon crystal, which will constitute the template for our Ar matrix and Ar surface in the following periodic calculations. Argon has a face centred cubic (fcc) lattice and we choose to use four Ar layers of 18 atoms each, thus leading to a cubic unit cell ($\alpha = \beta = \gamma = 90°$) containing 72 Ar atoms. Fujii and co-workers measured a lattice constant for a pure argon crystal of 5.2229 Å at zero temperature.[66] After optimization of our Ar crystal model, we obtain a lattice constant of 5.2226 Å, in good agreement with experimental data. Note that our PBE-D3 value is in better agreement with experimental data than the previous theoretical value of 5.354 Å obtained at the CCSD(T) level using a valence basis set (6s6p3d1f)/[4s4p3d1] supplemented with diffuse 1s1p1d1f

Table 4 Equilibrium structures of the CO–Ar$_3$ complex. Distances are in Å. Angles are in degrees. The binding energies and the harmonic vibrational frequencies are in cm^{-1}. In bold are the CO harmonic frequencies. The atoms were described using the aug-cc-pVTZ basis set

	Minimum 1			Transition state		Minimum 2	
	PBE-D3	MP2	CCSD(T)-F12	MP2	CCSD(T)-F12	MP2	CCSD(T)-F12
r	1.136	1.139	1.130	1.139	1.131	1.139	1.131
R_1	3.519	3.449	4.371	3.760	3.789	3.763	3.696
R_2	3.460	3.714	3.362	4.620	4.657	3.767	4.764
R_3	3.628	3.713	3.725	3.640	3.660	3.445	3.596
d_1	3.953	3.865	4.643	4.682	3.770	6.974	6.551
d_2	3.950	4.650	3.876	6.512	7.386	7.336	8.213
d_3	4.025	2.970	2.997	8.175	7.083	3.769	3.678
θ	97.9	137.9	35.6	77.5	76.5	77.4	85.8
α_1	68.9	63.1	71.0	112.2	113.4	154.3	57.8
α_2	67.0	63.1	56.4	164.9	165.9	143.0	131.9
E_B	−358.8	−317.9	−272.5	−154.3	−192.8	−173.0	−208.9
ω	**2145.6**	**2107.4**		**2106.6**		**2108.0**	
	431.6	50.0		63.5		50.7	
	428.1	41.2		38.6		40.0	
	329.7	36.3		32.5		39.1	
	37.7	35.0		30.0		34.9	
	33.3	27.7		22.3		26.6	
	29.1	27.1		21.5		26.3	
	24.1	19.4		3.2		13.0	
	21.9	19.3		i1.0		11.7	

This journal is © the Owner Societies 2015

Phys. Chem. Chem. Phys., 2015, **17**, 17159–17168 | **17163**

functions[67] and that obtained using ACFDT-PBE with a plane-wave based code (5.3 Å).[68] We note here that the inclusion of dispersion corrections seems to play a key role in obtaining good experimental agreement for the Ar crystal. Halo *et al.*[69] developed a periodic local MP2 program and used it to describe fcc rare gas crystals. Their study showed good results for homogeneous systems, leading to a lattice constant of 5.20 Å for the Ar crystal, yet their approach remains computationally costly.

2. CO in interaction with an Ar surface

For these computations, we used four argon layers, which are formed by 4×8 Ar atoms, using our optimised fcc structure (lattice constant: $a = 5.222$ Å and angles: $\alpha = \beta = \gamma = 90°$) and added ~ 20 Å of vacuum along the c direction ($a = b = 16.029$ Å, and $c = 35$ Å). In order to estimate relaxation effects, we perform three sets of calculations where the Ar layers are either fully frozen, only the first Ar layer is relaxed, or only the first two Ar layers are relaxed. We use different starting points in our geometry optimisations that span possible orientations of CO with respect to the surface (parallel, CO upright and OC upright). Our results are shown in Table 5 and Fig. 1.

We obtain three minima on the surface, namely CO parallel to the surface ($CO\|Ar_{72}$), CO perpendicular to the surface oxygen down ($CO–Ar_{72}$) and CO perpendicular to the surface carbon down ($OC–Ar_{72}$). The CO distances to the surface, binding energy, harmonic CO stretches and CO–surface angles are shown in Table 5.

The lowest-energy minimum for the adsorption on the frozen surface (4 layers fixed) and the surface model with a single free layer corresponds to a CO molecule with its carbon

atom pointing towards the Ar surface (C–Ar = 3.582 Å and C–Ar = 3.551 Å, respectively). However, when we allow the first two layers to relax, the lowest-energy minimum has now a much lower binding energy (-681 cm^{-1}) and corresponds to a CO molecule with its oxygen atom pointing towards the Ar surface (O–Ar = 3.870 Å).

This marked change highlights that CO-induced perturbations are not limited to the first layer. This is may be related to the weak nature of the interaction between CO–Ar and Ar–Ar within the matrix as both binding energies are similar (see earlier). These effects may be effective several angstroms away from the dopant. Consequently, we show here the importance of relaxing the rare gas atoms when studying the interaction of molecules with rare gas environments. Such effects were already noticed by Gerber and co-workers for iodine in the argon matrix[70] and by Haas and Samuni[71] who discussed several examples. For instance, Gerber and co-workers showed that four solvation layers (448 atoms) with at least two layers (72 atoms) being mobile were needed for converged results. Here we needed two more relaxed layers than I₂@Ar since CO is slightly polar. Therefore, this renders the use of small dynamical cells with rigid walls questionable for such computations.

We also observe that δ differs from $0°$ or $90°$ due to the competition between favourable interactions between the outermost σ molecular orbital of CO and the Ar orbitals of the surface (leading to perpendicular CO *i.e.* $\delta = 90°$) and between the π orbital of CO and the Ar orbitals (leading to CO parallel to the surface *i.e.* $\delta = 0°$). A similar behaviour was noticed for imidazole and histidine interacting with the gold Au(111) surface.[72,73]

Finally, we show that the harmonic frequency decreases for both OC–Ar₇₂ and CO–Ar₇₂ when we release layers 1 and 2 (from 2144.2 cm^{-1} to 2140.2 cm^{-1} and from 2152.1 cm^{-1} to 2150.5 cm^{-1}, respectively). In contrast, for the less stable arrangement ($CO\|Ar_{72}$), we do not observe this systematic lowering of the harmonic frequency. Instead, releasing the first layer causes a 13.5 cm^{-1}drop in the CO frequency, but the releasing two layers leads to an increase of the CO stretch frequency to 2145.0 cm^{-1}.

3. Carbon monoxide embedded in an argon matrix

In order to assess the effect of matrix embedding, we use our optimised Ar crystal and replace one Ar atom in the centre of the unit cell by a CO molecule. This procedure ensures that the diatomic is fully enclosed in a periodic Ar environment. The results of the optimisations of both embedded CO and the periodic Ar matrix are depicted in Fig. 2 and shown in Table 6.

Four different unit cells were used to assess size effects: CO@Ar₃₁ ($2 \times 2 \times 2$ unit cell), CO@Ar₄₇ ($3 \times 2 \times 2$ unit cell), CO@Ar₇₄ ($3 \times 3 \times 2$ unit cell) and CO@Ar₁₀₇ ($3 \times 3 \times 3$ unit cell). Firstly, we note that, upon embedding, the CO equilibrium distance remains practically unchanged. In contrast to this, we observe that the position of CO within the matrix depends on the size of the matrix model. Table 6 shows that the average distance between CO and the argon atoms decreases as the cell size increases (from about 3.8 Å down to 3.4 Å).
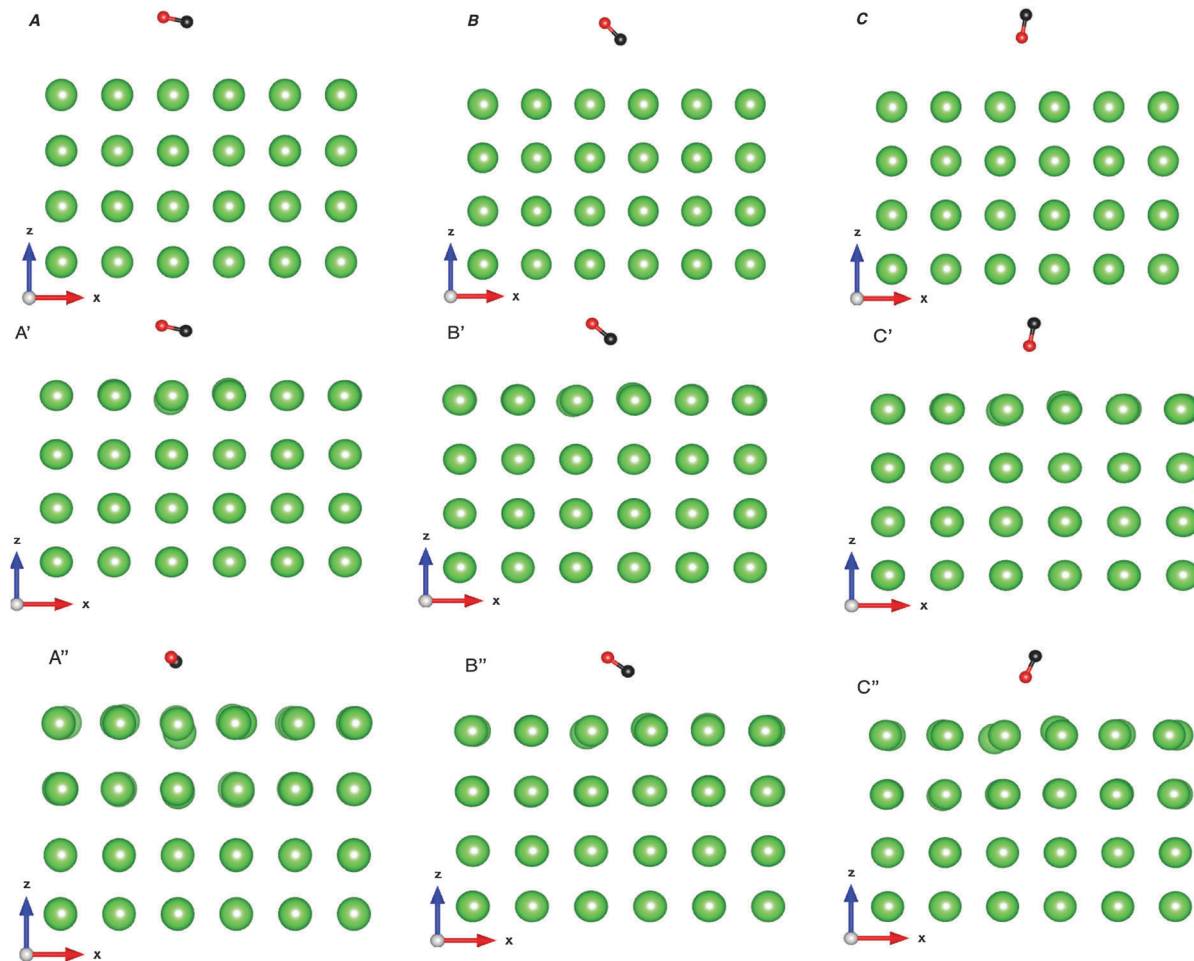
Table 5 Characteristics of the interaction of CO with an argon surface. *D* (in Å) are the distances between the C/O atoms of CO to the closest Ar of the surface. The BSSE-uncorrected binding energies (E_B) and the harmonic vibrational frequencies (ω_{CO}) are in cm^{-1}. Finally δ is the tilt angle in degrees of the molecular axis of the CO molecule with respect to the Ar surface

Number of frozen Ar layers	*D*	E_B	ω_{CO}	δ
CO‖Ar₇₂				
All layers	Ar–O = 3.744	−421.1	2144.7	9
	Ar–C = 3.546			
Bottom 3 layers	Ar–O = 3.697	−460.1	2131.2	10
	Ar–C = 3.488			
Bottom 2 layers	Ar–O = 3.470	−513.8	2145.0	8
	Ar–C = 3.606			
OC–Ar₇₂				
All layers	Ar–O = 4.125	−465.9	2144.2	47
	Ar–C = 3.582			
Bottom 3 layers	Ar–O = 3.966	−547.5	2142.0	45
	Ar–C = 3.551			
Bottom 2 layers	Ar–O = 3.800	−596.3	2140.2	43
	Ar–C = 3.539			
CO–Ar₇₂				
All layers	Ar–O = 3.560	−449.5	2152.1	86
	Ar–C = 4.700			
Bottom 3 layers	Ar–O = 3.448	−527.7	2151.9	83
	Ar–C = 4.571			
Bottom 2 layers	Ar–O = 3.870	−680.8	2150.5	66
	Ar–C = 4.523			

17164 | *Phys. Chem. Chem. Phys.,* 2015, **17**, 17159–17168

This journal is © the Owner Societies 2015

Fig. 1 Equilibrium geometry of CO in interaction with an Ar surface. A: CO∥Ar$_{72}$(frozen), A′: CO∥Ar$_{72}$(3 layers frozen), A″: CO∥Ar$_{72}$(2 layers frozen). B: OC−Ar$_{72}$(frozen), B′: OC−Ar$_{72}$(3 layers frozen), B″: OC−Ar$_{72}$(2 layers frozen). C: CO−Ar$_{72}$(frozen), C′: CO−Ar$_{72}$(3 layers frozen), and C″: CO−Ar$_{72}$(2 layers frozen). See Table 5 for more details.

It is also noteworthy that the arrangement of Ar atoms at the surface near the CO molecule is not dissimilar to those seen in CO–Ar$_2$ or CO–Ar$_3$. Thus we can conclude that most stable clusters detailed in Tables 3 and 4 are very similar to CO attached to the surface of a large Ar cluster as pointed out by Paesani *et al.*[47]

Table 6 shows that there is a slight decrease in the CO harmonic vibrational frequency from 2153.5 cm^{-1} for isolated CO to $\sim$2135 cm^{-1} for CO embedded in a matrix made of 74 or 107 argon atoms per unit cell. The smaller CO@Ar$_{31}$ matrix leads to an intermediate CO stretching frequency of $\sim$2140 cm^{-1}. As can be inferred from Fig. 2a, the unit cell containing 31 Ar atoms is very small and there are less than 4 Ar layers that separate CO from its periodic image. This leads to a "CO–CO" distance of 10.77 Å and lateral interactions could be the cause for the intermediate harmonic frequency value. Indeed, in Section IV.2, we have shown that CO creates a strong perturbation in the Ar layers and thus 31 Ar atoms might not be enough to screen the induced perturbations of CO in the matrix. For cells containing 47 Ar atoms or more, the separation between CO and its image is larger than 12.24 Å and the harmonic CO stretch appears to be converged. This would imply that the

CO-induced perturbations are more effectively screened so that we may consider the CO fully solvated in those unit cells. For Na$_2$ embedded in an argon matrix, Groβ and Spiegelmann[74] noticed similar effects. However, we note that for H$_2$@Ar, these effects are reduced (see ESI†). Indeed, due to the smaller size of the molecule, a cell of 31 Ar atoms is sufficient to fully solvate H$_2$ unlike CO. This difference may also be related to the weaker interaction between H$_2$ and Ar compared to CO–Ar. As H$_2$ is non-polar whereas CO is polar we can infer that the interaction potential of CO with Ar should be deeper and extends to longer ranges for CO–Ar in contrast to the one between H$_2$ and Ar. Indeed, the binding energy is of the order of $\sim$−50 cm^{-1} for H$_2$–Ar[75] compared to more than −100 cm^{-1} for CO–Ar. As said above, this is also in line with the finding of Gerber and co-workers for iodine in an argon matrix[70] and of Haas and Samuni.[71]

Because of the importance of the Basis Set Superposition Error in these types of systems (weak binding), we report here only BSSE-corrected binding energies. To explore basis set effects, we calculate the BSSE using two different basis sets: a triple-zeta basis set and a quadruple-zeta basis set. With a triple zeta basis set, we observe a large CP-correction as the value of the binding energy decreases to
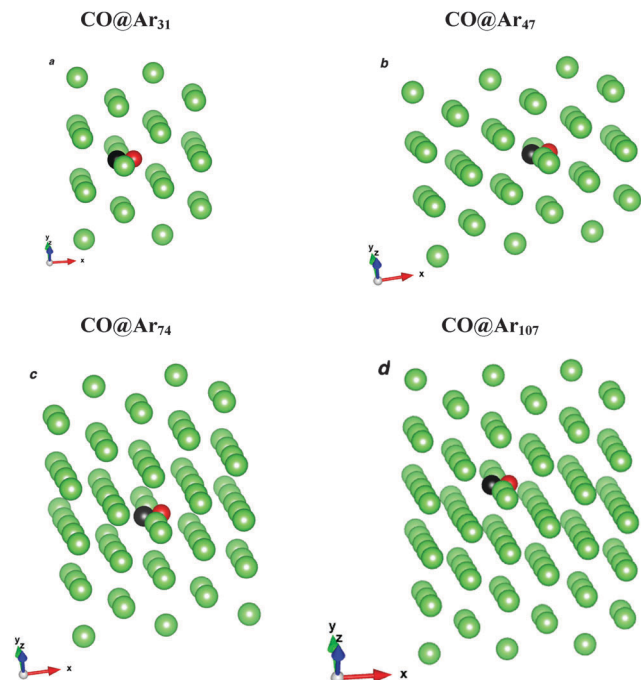
This journal is © the Owner Societies 2015

Phys. Chem. Chem. Phys., 2015, **17**, 17159–17168 | **17165**

Fig. 2 Equilibrium geometries of CO embedded into Ar matrices of different sizes.

Table 6 Characteristics of CO embedded into Ar matrices. R_{CO} (in Å) is the CO equilibrium distance. ω_{CO} (in cm^{-1}) is the CO harmonic frequency. $\Delta\omega_{CO}$ (in cm^{-1}) is the difference between the harmonic frequency of isolated CO and that of CO embedded into Ar matrices. We also report in angstroms the average distance between the carbon atom of CO and the 12 closest neighbouring Ar atoms ($\langle$C–Ar$\rangle$) and a similar quantity of the oxygen atoms of CO ($\langle$O–Ar$\rangle$). The distance between CO and its periodic image is given in angstroms

Molecular system	R_{CO}	ω_{CO}	Δw_{CO}	$\langle$C–Ar$\rangle$	$\langle$O–Ar$\rangle$	CO–CO distance
CO	1.137	2153.5	—	—	—	—
	1.128[a]	2169.8[a]				
CO@Ar$_{31}$	1.1379	2140.1	13.4	3.807	3.830	10.77
CO@Ar$_{47}$	1.1377	2134.6	18.9	3.806	3.916	12.24
CO@Ar$_{74}$	1.1374	2134.6	18.9	3.731	3.785	14.36
CO@Ar$_{107}$	1.1376	2134.6	18.9	3.730	3.489	15.67
CO@Ar[b]	—	2140.1	29.7	—	—	—

[a] Exp. ref. 81. [b] Exp. ref. 77.

641.26 cm^{-1} upon BSSE correction (almost 58.87%, $E_{B(BSSE\text{-}corrected)}$ = -918.06 cm^{-1} and $E_{B(BSSE\text{-}UNcorrected)}$ = -1559.32 cm^{-1}). In contrast, when we use a quadruple zeta basis, the BSSE correction decreased to 2.93%, leading to a BSSE-corrected value of $E_{B(BSSE\text{-}corrected)}$ = -988.95 cm^{-1} compared to the uncorrected value of $E_{B(BSSE\text{-}UNcorrected)}$ = -1018.89 cm^{-1}.

V. General trends

1. Binding energy evolution upon complex formation and solvation

Our systematic study of the interaction of CO with Ar in various environments shows that as the number of argons surrounding the CO molecule increases so does the binding energy. For CO–Ar we compute a binding energy of ~ -130 to -150 cm^{-1}. For CO–Ar$_2$, we compute an E_B per Ar atom of ~ -130 to -135 cm^{-1}, and ~ -120 cm^{-1} per Ar atom for CO–Ar$_3$. When CO interacts with our Ar surface, six Ar atoms are influenced in the binding, which leads to a binding energy per Ar atom of ~ -135 cm^{-1}. In the matrix, CO has 12 neighbouring argon atoms leading to ~ -125 cm^{-1} per Ar atom. Interestingly, our calculations show that the binding energy per Ar atom is almost constant at ~ -130 cm^{-1} per Ar atom independent of the environment of the CO molecule. Since the size of the Ar atom and the CO molecule are similar and since this energy is close to the Ar–Ar interaction of ~ -100 cm^{-1},[76] replacing an Ar atom in the Ar matrix with a CO molecule causes only limited perturbations in these media, as noticed above.

2. Complex formation and embedding induced CO vibrational shifts

The harmonic vibrational frequency of carbon monoxide decreases linearly as the number of attached Ar atoms increases before reaching a plateau for CO embedded into the matrix. Indeed, the CO harmonic vibrational frequency diminishes by -2.9, -6.4, -7.9 cm^{-1} for CO–Ar$_n$ ($n = 1$, 2, and 3), by -7.3 cm^{-1} for CO in interaction with the Ar surface; and by -13.4, -18.9 cm^{-1} for CO@Ar$_{31}$ and CO@Ar$_{\geq 47}$, respectively. Experimentally, the CO frequency shift upon embedding in an Ar matrix is -29.7 cm^{-1}.[77] The observed trend for the evolution of our computed CO shift is in agreement with this value. Deviations from the experiment may be due to the following reasons: (i) we use a perfect argon crystal (fcc), while in experiments the rare gas structure might differ from that of a crystalline solid; (ii) we have not taken into account anharmonicity effects that may be relevant for such weakly bond entities. It is also worth noting that such vibrational shifts were already observed for other molecules embedded in Ar matrices, such as HCl@Ar[78] and HF@Ar.[79]

VI. Conclusions

We observe a gradual change in the vibrational frequency of CO as the number of interacting Ar atoms is increased from the cluster regime up to full matrix embedding. This effect is rationalized in terms of equivalent bimolecular interaction potentials between CO–Ar and Ar–Ar entities. In addition, we show convergence of the vibrational frequency once we reach full embedding in a matrix.

Our benchmark study of these CO@Ar$_n$ species highlights that dispersion-corrected DFT provides an efficient and reliable framework to describe weak interactions between small molecules and rare gas systems. From a technical point of view, we see that Grimme's PBE-D3 approach provides an accurate description of molecules interacting with rare gases. In this context, PBE-D3 provides a uniform formalism for the treatment of molecules in a gas phase, adsorbed on a surface or in the solid state and thus enables one-to-one comparisons, which

17166 | *Phys. Chem. Chem. Phys.*, 2015, **17**, 17159–17168

This journal is © the Owner Societies 2015

would not be easily feasible using traditional wave function methods.

Our periodic approach to matrix embedding addresses a number of issues seen in cluster techniques, such as asymmetry of the embedding environment, and allows better estimation of size effects. However, care has to be taken in the periodic approach to ensure a sufficient dilution (a ratio between the solute and embedding rare gas) and we show how these dilution effects can impact the vibrational frequency. This also implies that cautions should be exercised when comparing spectroscopic data obtained using matrix embedding to measurements in the gas-phase or to theoretical data.

Finally, our embedding technique allows us to perform a deeper analysis of local embedding sites, which is mandatory for a realistic modelling of the surrounding matrix environments and for determining matrix shifts, as noticed recently by K. Niimi et al.[9]

Our approach is currently being further developed in our laboratories to investigate embedding of other solutes (e.g. N_2, NO, CO_2...) relevant to atmospheric and environmental studies.

Acknowledgements

References

1 G. C. Pimental and S. W. Charles. pac.iupac.org/publications/pac/7/1/0111/pdf/.

2 V. Barone, M. Biczyskoa and J. Bloino, *Phys. Chem. Chem. Phys.*, 2014, **16**, 1759.

3 H. Friedmann and S. Kimel, *J. Chem. Phys.*, 1965, **43**, 3925.

4 Z. Bihary, R. B. Gerber and V. A. Apkarian, *J. Chem. Phys.*, 2001, **115**, 2695.

5 J. Kalinowski, R. B. Gerber, M. Räsänen, A. Lignell and L. Khriachtchev, *J. Chem. Phys.*, 2014, **140**, 094303.

6 G. Liu, Y. Zhang, Z. Wang, Y. Wang, X. Zhang and W. Zhang, *Comput. Theor. Chem.*, 2012, **993**, 118.

7 G. Liu, W. Zhang, X. Zhang, T. He and J. Cheng, *Comput. Theor. Chem.*, 2014, **1028**, 46.

8 C. Fabri, T. Szidarovszky, G. Magyarfalvi and G. Tarczay, *J. Phys. Chem. A*, 2011, **115**, 4640.

9 K. Niimi, A. Nakayama, Y. Ono and T. Taketsugu, *J. Phys. Chem. A*, 2014, **118**, 380.

10 A. Vargas, N. Bonalumi, D. Ferri and A. Baiker, *J. Phys. Chem. A*, 2006, **110**, 1118–1127.

11 T. S. Zwier, *Annu. Rev. Phys. Chem.*, 1996, **47**, 205–241.

12 J. A. Hogendoorn, W. P. M. van Swaaij and G. F. Versteeg, *J. Chem. Eng.*, 1995, **59**, 243–252.

13 B. Olas, *Chem.-Biol. Interact.*, 2014, **222**, 37–43.

14 I. Tobias, R. J. Fallon and J. T. Vandersllce, *J. Chem. Phys.*, 1960, **33**, 1638–1640.

15 J. N. Huffaker, *J. Mol. Spectrosc.*, 1977, **65**, 1–19.

16 C. G. Diaz and R. H. Tapping, *J. Mol. Spectrosc.*, 1994, **163**, 58–66.

17 Y. F. Liu, Y. Jia, D. H. Shi, J. F. Sun and J. Quanti, *J. Quant. Spectrosc. Radiat. Transfer*, 2011, **112**, 2296–2302.

18 Y. Xu and R. W. McKellar, *Mol. Phys.*, 1996, **88**, 859.

19 R. R. Toczyłowski and S. M. Cybulski, *J. Chem. Phys.*, 2000, **112**, 4640.

20 H. J. Castejón, M. C. Salazar, J. L. Paz and A. J. Hernández, *J. Mol. Struct.*, 2006, **801**, 1–5.

21 G. D. Purvis III and R. J. Bartlett, *J. Chem. Phys.*, 1982, **76**, 1910–1918.

22 M. Havenith and G. W. Schwaab, *Z. Phys. Chem.*, 2005, **219**, 1053–1088.

23 B. Kukawska-Tarnawska, G. Chalasinski and K. Olszewski, *J. Chem. Phys.*, 1994, **101**, 4964–4974.

24 C. Møller and M. S. Plesset, *Phys. Rev.*, 1934, **46**, 618.

25 L. A. Curtiss, P. C. Redfern, K. Raghavachari, V. Rassolov and J. A. Pople, *J. Chem. Phys.*, 1999, **110**, 4703.

26 P. J. Knowles, J. S. Andrews, R. D. Amos, N. C. Handy and J. A. Pople, *Chem. Phys. Lett.*, 1991, **186**, 130.

27 P. J. Knowles and H.-J. Werner, *Chem. Phys. Lett.*, 1985, **115**, 259–267.

28 H.-J. Werner and P. J. Knowles, *J. Chem. Phys.*, 1985, **82**, 5053–5063.

29 H.-J. Werner and P. J. Knowles, *J. Chem. Phys.*, 1988, **89**, 5803–5814.

30 P. J. Knowles and H.-J. Werner, *Chem. Phys. Lett.*, 1988, **145**, 514–522.

31 P. J. Knowles, C. Hampel and H.-J. Werner, *J. Chem. Phys.*, 1993, **99**, 5219.

32 P. J. Knowles, C. Hampel and H.-J. Werner, *J. Chem. Phys.*, 2000, **112**, E3106.

33 G. Knizia, T. B. Adler and H. Werner, *J. Chem. Phys.*, 2009, **130**, 054104.

34 H. J. Werner, P. J. Knowles, G. Knizia, F. R. Manby, M. Schütz, P. Celani, T. Korona, R. Lindh, A. Mitrushenkov, G. Rauhut, K. R. Shamasundar, T. B. Adler, R. D. Amos, A. Bernhardsson, A. Berning, D. L. Cooper, M. J. O. Deegan, A. J. Dobbyn, F. Eckert, E. Goll, C. Hampel, A. Hesselmann, G. Hetzer, T. Hrenar, G. Jansen, C. Köppl, Y. Liu, A. W. Lloyd, R. A. Mata, A. J. May, S. J. McNicholas, W. Meyer, M. E. Mura, A. Nicklass, D. P. O'Neill, P. Palmieri, D. Peng, K. Pflüger, R. Pitzer, M. Reiher, T. Shiozaki, H. Stoll, A. J. Stone, R. Tarroni, T. Thorsteinsson and M. Wang, MOLPRO-2012-1, 2012.

35 M. J. Frisch, G. W. Trucks, H. B. Schlegel, G. E. Scuseria, M. A. Robb, J. R. Cheeseman, G. Scalmani, V. Barone, B. Mennucci, G. A. Petersson, H. Nakatsuji, M. Caricato, X. Li, H. P. Hratchian, A. F. Izmaylov, J. Bloino, G. Zheng, J. L. Sonnenberg, M. Hada, M. Ehara, K. Toyota, R. Fukuda, J. Hasegawa, M. Ishida, T. Nakajima, Y. Honda, O. Kitao, H. Nakai, T. Vreven, J. A. Montgomery Jr., J. E. Peralta, F. Ogliaro, M. Bearpark, J. J. Heyd, E. Brothers, K. N.

This journal is © the Owner Societies 2015

Phys. Chem. Chem. Phys., 2015, **17**, 17159–17168 | **17167**

Kudin, V. N. Staroverov, R. Kobayashi, J. Normand, K. Raghavachari, A. Rendell, J. C. Burant, S. S. Iyengar, J. Tomasi, M. Cossi, N. Rega, J. M. Millam, M. Klene, J. E. Knox, J. B. Cross, V. Bakken, C. Adamo, J. Jaramillo, R. Gomperts, R. E. Stratmann, O. Yazyev, A. J. Austin, R. Cammi, C. Pomelli, J. W. Ochterski, R. L. Martin, K. Morokuma, V. C. Zakrzewski, G. A. Voth, P. Salvador, J. J. Dannenberg, S. Dapprich, A. D. Daniels, Ö. Farkas, J. B. Foresman, J. V. Ortiz, J. Cioslowski and D. J. Fox, Gaussian 09, Revision D.01, 2009.

36 T. H. Dunning, *J. Chem. Phys.*, 1989, **90**, 1007–1023.

37 R. A. Kendall, T. H. Dunning Jr. and R. J. Harrison, *J. Chem. Phys.*, 1992, **96**, 6796–6806.

38 D. E. Woon and T. H. Dunning Jr., *J. Chem. Phys.*, 1993, **98**, 1358–1371.

39 D. E. Woon and T. H. Dunning Jr., *J. Chem. Phys.*, 1995, **103**, 4572–4585.

40 W. Klopper, *Mol. Phys.*, 2001, **99**, 481.

41 F. Weigend, A. Kohn and C. Hattig, *J. Chem. Phys.*, 2002, **116**, 3175.

42 K. E. Yousaf and K. A. Peterson, *Chem. Phys. Lett.*, 2009, **476**, 303.

43 F. Lique, J. Klos and M. Hochlaf, *Phys. Chem. Chem. Phys.*, 2010, **12**, 15672.

44 K. Mathivon, R. Linguerri and M. Hochlaf, *J. Chem. Phys.*, 2013, **139**, 164306.

45 Y. Ajili, K. Hammami, N. E. Jaidane, M. Lanza, Y. N. Kalugina, F. Lique and M. Hochlaf, *Phys. Chem. Chem. Phys.*, 2013, **15**, 10062.

46 P. Hohenberg and W. Kohn, *Phys. Rev.*, 1964, **136**, B864.

47 F. Paesani, F. A. Gianturco, M. Lewerenz and J. P. Toennies, *J. Chem. Phys.*, 1999, **111**, 6897.

48 J. A. Snyder, D. R. Alfonso, J. E. Jaffe, Z. Lin, A. C. Hess and M. Gutowski, *J. Phys. Chem. B*, 2000, **104**, 4717.

49 G. R. B. Gomes and J. A. N. F. Gomes, *Surf. Sci.*, 1999, **503**, 189–200.

50 J. M. Pérez-Jordá and A. D. Becke, *Chem. Phys. Lett.*, 1995, **233**, 134–137.

51 J. M. Pérez-Jordá, E. San-Fabían and A. J. Pérez-Jiménez, *J. Chem. Phys.*, 1999, **110**, 1916–1920.

52 (*a*) S. Grimme, J. Antony, S. Ehrlich and H. Krieg, *J. Chem. Phys.*, 2010, **132**, 154104; (*b*) W. Reckien, F. Janetzko, M. F. Peintinger and T. Bredow, *J. Comput. Chem.*, 2012, **33**, 2023–2031; (*c*) S. Ehrlich, J. Moellmann, W. Reckien, T. Bredow and S. Grimme, *ChemPhysChem*, 2011, **12**, 3414–3420.

53 J. G. Ángyán, I. C. Gerber, A. Savin and J. Toulouse, *Phys. Rev. A: At., Mol., Opt. Phys.*, 2005, **72**, 012510.

54 O. Kullie and T. Saue, *Chem. Phys.*, 2012, **395**, 54–62.

55 J. VandeVondele, M. Krack, F. Mohamed, M. Parrinello, T. Chassaing and H. Hutter, *Comput. Phys. Commun.*, 2005, **167**, 103–128.

56 C. J. Mundy, F. Mohamed, F. Schiffman, G. Tabacchi, H. Forbert, W. Kuo, J. Hutter, M. Krack, M. Iannuzzi, M. McGrath, M. Guidon, T. D. Kuehne, T. Laino, J. VandeVondele and V. Weber, *CP2K software package*, Version 2.4, 2013, http://cp2k.berlios.de.

57 S. Goedecker, M. Teter and J. Hutter, *Phys. Rev. B: Condens. Matter Mater. Phys.*, 1996, **54**, 1703–1710.

58 X. Xu and W. A. Goddardlll, *J. Chem. Phys.*, 2004, **121**, 4068.

59 J. VandeVondele and J. Hutter, *J. Chem. Phys.*, 2007, **127**, 114105.

60 B. Liu and A. D. McLean, *J. Chem. Phys.*, 1973, **59**, 4557.

61 S. F. Boys and F. Bernardi, *Mol. Phys.*, 1970, **19**, 553–566.

62 R. Hilal, W. M. I. Hassan, S. A. K. Elroby and S. G. Aziz, *Procedia Computer Science*, 2013, **18**, 826–834.

63 Y. Sumiyoshi and Y. Endo, *J. Chem. Phys.*, 2015, **142**, 024314.

64 J. F. Ogilvie and Y. H. Wang, *J. Mol. Struct.*, 1992, **273**, 277–290.

65 P. Slavíček, R. Kalus, P. Paška, I. Odvárková, P. Hobza and A. Malijevský, *J. Chem. Phys.*, 2013, **119**, 2102.

66 Y. Fujii, N. A. Lurie, R. Prynn and G. Shirane, *Phys. Rev. B: Condens. Matter Mater. Phys.*, 1974, **10**, 3647.

67 K. Rosciszewsk, B. Paulus, P. Fulde and H. Stoll, *Phys. Rev. B: Condens. Matter Mater. Phys.*, 2000, **62**, 5482.

68 J. Harl and G. Kresse, *Phys. Rev. B: Condens. Matter Mater. Phys.*, 2008, **79**, 045136.

69 M. Halo, S. Casassa, L. Maschio and C. Pisani, *Chem. Phys. Lett.*, 2009, **467**, 294–298.

70 Z. Bihary, R. B. Gerber and V. A. Apkarian, *J. Chem. Phys.*, 2001, **115**, 2695.

71 Y. Haas and U. Samuni, *Prog. React. Kinet.*, 1998, **23**, 211–280.

72 M. Prakash, K. Mathivon, D. M. Benoit, G. Chambaud and M. Hochlaf, *Phys. Chem. Chem. Phys.*, 2014, **16**, 12503–12509.

73 F. Iori, S. Corni and R. Di Felice, *J. Phys. Chem. C*, 2008, **112**, 13540–13545.

74 M. Groß and F. Spiegelmann, *J. Chem. Phys.*, 1998, **108**, 4148.

75 R. J. Le Roy and J. M. Hutson, *J. Chem. Phys.*, 1987, **86**, 837.

76 R. A. Aziz, *J. Chem. Phys.*, 1993, **99**, 4158.

77 H. Abe, H. Takeo and K. M. T. Yamada, *Chem. Phys. Lett.*, 1999, **311**, 153–158.

78 D. T. Anderson, S. Davis and D. J. Nesbitt, *J. Chem. Phys.*, 1997, **107**, 4.

79 S. Liu, Z. Bacic and J. W. Moskowitz, *J. Chem. Phys.*, 1994, **101**, 181.

80 Data base Cccbdb.nist.gov.

81 K. P. Huber and G. Herzberg, *Molecular Spectra and Molecular Structure.IV*, Constants of Diatomic MoleculesNew York, Reinhold, 1979.

82 V. Castells, N. Halberstadt, S. K. Shin, R. A. Beaudet and C. Wittig, *J. Chem. Phys.*, 1994, **101**, 1006.

83 S. Shin, S. K. Shin and F.-M. Tao, *J. Chem. Phys.*, 1996, **104**, 183.

84 J. A. Warren, G. R. Smith and W. A. Guillory, *J. Chem. Phys.*, 1980, **72**, 4901.

17168 | *Phys. Chem. Chem. Phys.*, 2015, **17**, 17159–17168

This journal is © the Owner Societies 2015